IOP PUBLISHING JOURNAL OF PHYSICS D: APPLIED PHYSICS

J. Phys. D: Appl. Phys. **45** (2012) 485101 (7pp) doi:10.1088/0022-3727/45/48/485101

Near-field interactions in electric inductive–capacitive resonators for metamaterials

Withawat Withayachumnankul, Christophe Fumeaux and Derek Abbott

School of Electrical and Electronic Engineering, The University of Adelaide, Adelaide, SA 5005, Australia

E-mail: withawat@eleceng.adelaide.edu.au

Received 27 June 2012, in final form 18 September 2012
Published 6 November 2012
Online at stacks.iop.org/JPhysD/45/485101

Abstract

Near-field interactions in an array of electric inductive–capacitive (ELC) resonators are investigated analytically, numerically and experimentally. The measurement and simulation results show that inter-cell coupling plays an important role in determining the response of metamaterials. A quasistatic dipole–dipole interaction model, together with a Lagrangian formalism, quantitatively explains the interplay between the electric and magnetic couplings in the resonator array. Depending on the alignment of the resonators, the couplings can cause resonance shifting and/or splitting. The knowledge obtained from this study is crucial in designing metamaterials with ELC resonators.

(Some figures may appear in colour only in the online journal)

1. Introduction

A metamaterial defines a group of resonators that collectively exhibit a strong electric and/or magnetic resonance. Examples of such resonators include split-ring resonators (SRRs) [1], (electric inductive-capacitor (ELC)) resonators [2, 3] and fishnets [4]. These resonators typically operate in the *effective medium* regime owing to their subwavelength physical dimensions. Their response is therefore characterized by the effective permittivity and permeability, which can be controlled via the shape, size and material characteristics of the resonators.

As important as the geometry and constituent materials is near-field coupling between the resonators that also plays a role in determining the response of metamaterials. The resonance hybridization due to near-field interactions in metamaterials leads to new phenomena, including resonance splitting and band broadening [5]. A Lagrangian formalism with a quasistatic dipole–dipole interaction model [5, 6] has been successfully used to study the hybridization effects in SRR dimers [7–9] SRR chains [10, 11] and SRR arrays [12–14]. In these resonator systems, it is found that both electric and magnetic dipoles contribute to inter-resonator coupling, and the coupling efficiency depends on the distance and relative orientation among the resonators [5].

An ELC resonator was proposed as a route to metamaterials with customizable values of the permittivity [2, 3]. These resonators, in conjunction with SRRs that provide negative permeability, can be used to construct a negative-index material [15, 16]. The unconventional electromagnetic properties of ELC resonators have been exploited in many other types of devices, e.g., absorbers [17, 18], reflectors [19], modulators [20, 21], polarizers [22, 23] and wave plates [24]. The implementation of ELC resonators in a wide range of applications necessitates the insight into their near-field behaviour. Understanding the coupling between nearby resonators will help towards engineering desirable responses.

A major difference between an ELC resonator and an SRR is the structural symmetry that significantly influences their field distributions and dipole moments. Specifically, the mirror symmetry in an ELC resonator prohibits the magnetic and magnetoelectric inductions that take place in SRRs [2]. The implication is a remarkable difference in inter-cell coupling behaviours. Hence, the knowledge acquired from those earlier studies on the SRR hybridization is not directly applicable to ELC resonators. As such, this paper presents a study on near-field interactions in 3D ELC-resonator arrays. The study begins with lateral coupling in planar resonators in

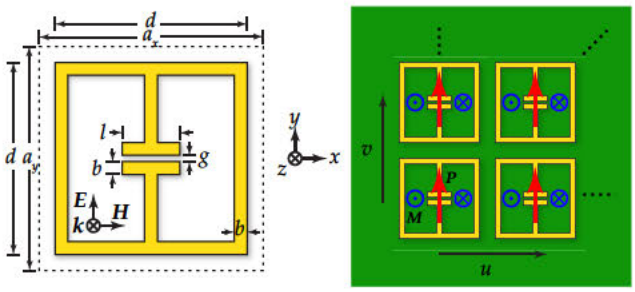

(a) single ELC resonator (b) ELC resonator array

Figure 1. ELC resonators. (*a*) A unit cell with dimensions as follows: $g = 0.3$ mm, $b = 0.4$ mm, $l = 1.8$ mm and $d = 4$ mm. (*b*) An array of ELC resonators. The electric dipoles (red arrows) are in plane and perpendicular to the gaps, whilst the magnetic dipoles (blue arrows) are out of plane.

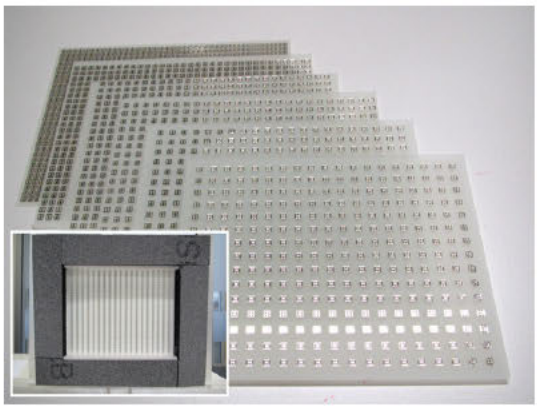

Figure 2. Fabricated metamaterials with different periodicities. Each metamaterial is composed of an array of ELC resonators on an FR4 substrate. The periodicity of the arrays is varied in order to experimentally observe the effect of coupling in the transverse directions. The inset shows a metamaterial positioned in the holder. The absorber frame prevents microwave diffraction around the edges of the sample.

section 2. It then extends to the coupling effects in the stacked resonators, or ELC dimers, in section 3. The coupling mechanisms will be explained through a dipole interaction model and Lagrangian description. The results clearly show unique coupling behaviours in the symmetric resonators.

2. Transversal coupling

2.1. Observation

The transversal or in-plane coupling among planar ELC resonators is considered in this section. A schematic diagram of a unit cell is shown in figure 1(*a*). In order to study the coupling effects, the lattice constants a_x and a_y are varied between 5 and 10 mm with a step size of 1 mm. An array of the resonators is fabricated on an epoxy FR4 substrate with a thickness of 0.8 mm, a measured dielectric constant of 4.0 and a reported loss tangent of 0.02. The metal used for the resonators is gold-coated copper with a copper thickness of 35 μm. The resonator array gives the first-order resonance in the microwave X band, i.e. 8–12 GHz. Shown in figure 2, the total board dimensions are 160 mm 190 mm, which is large enough to span across the main beam of a nearby feeding horn antenna.

The measurement is carried out in an anechoic chamber with a pair of microwave horn antennas as transmitting and receiving ports, separated by 5 m. The array is placed 50 mm away from the horn aperture of the receiving antenna to cover the receiving beamwidth. The sample transmission is measured and compared with the free-space transmission. The experimental configuration is not ideal because of the plane-wave approximation and the finite size of the array in the lateral directions. As a supplement, the simulation with ideal conditions is performed using CST Microwave Studio. Unit-cell boundary conditions are utilized for the transverse boundaries to replicate an infinite planar array of resonators. Two Floquet ports facing the array allow determining its response to a plane wave incident normally.

Figure 3 depicts the simulated and measured transmission profiles for the arrays with different lattice constants. The results from simulation and measurement are in general agreement. In figures 3(*a*) and (*b*), as the horizontal lattice constant decreases, a small change in the resonance frequency is observed, i.e., approx 0.5% of the initial value. From figures 3(*c*) and (*d*) a large redshift can be observed as the vertical lattice constant decreases. In the case of a square lattice in figures 3(*e*) and (*f*), the decreasing lattice constants cause a redshift in the resonance.

A change in the resonance frequency can be described by the dipole–dipole interaction model, illustrated in figure 1(*b*). A nearly constant resonance frequency as a_x varies in figures 3(*a*) and (*b*) can be attributed to the counteraction between the transversely coupled electric and magnetic dipoles in the horizontal direction. The electric dipoles are parallel and in phase and hence tend to shift the resonance upwards, but the effect is weakened by the magnetic dipoles that are anti-phase. On the other hand, a large resonance redshift as a_y decreases in figures 3(*c*) and (*d*) is caused by longitudinal coupling of the in-phase electric dipoles in the vertical direction. Likewise, a redshift as a_x and a_y decrease in figures 3(*e*)and (*f*) is mainly caused by the longitudinal electric dipole coupling. In all of the cases, as the lattice constants decrease, the resonance is broadened and the effective extinction cross section (not shown) is reduced. These effects are from enhanced scattering in strongly coupled dipoles [14].

2.2. Analysis

The near-field interactions among the in-plane resonators can be quantitatively explained on the basis of a quasistatic approximation [9, 14], in which the free-space wavelength is considered to be much longer than the interaction length. In an uncoupled resonator, the electrostatic and kinetic energies stored in the capacitive gap and inductive loop are given as, respectively, $Q^2/2C$ and $L\dot{Q}^2/2$. Here, Q is the charge, $\dot{Q} = \mathrm{d}Q/\mathrm{d}t$ is the current and L and C are the distributed inductance and capacitance. Given that $Q_{u,v}$ and $\dot{Q}_{u,v}$, respectively, denote the total charge and current in the uvth resonator, the Lagrangian for a planar array of coupled ELC resonators can

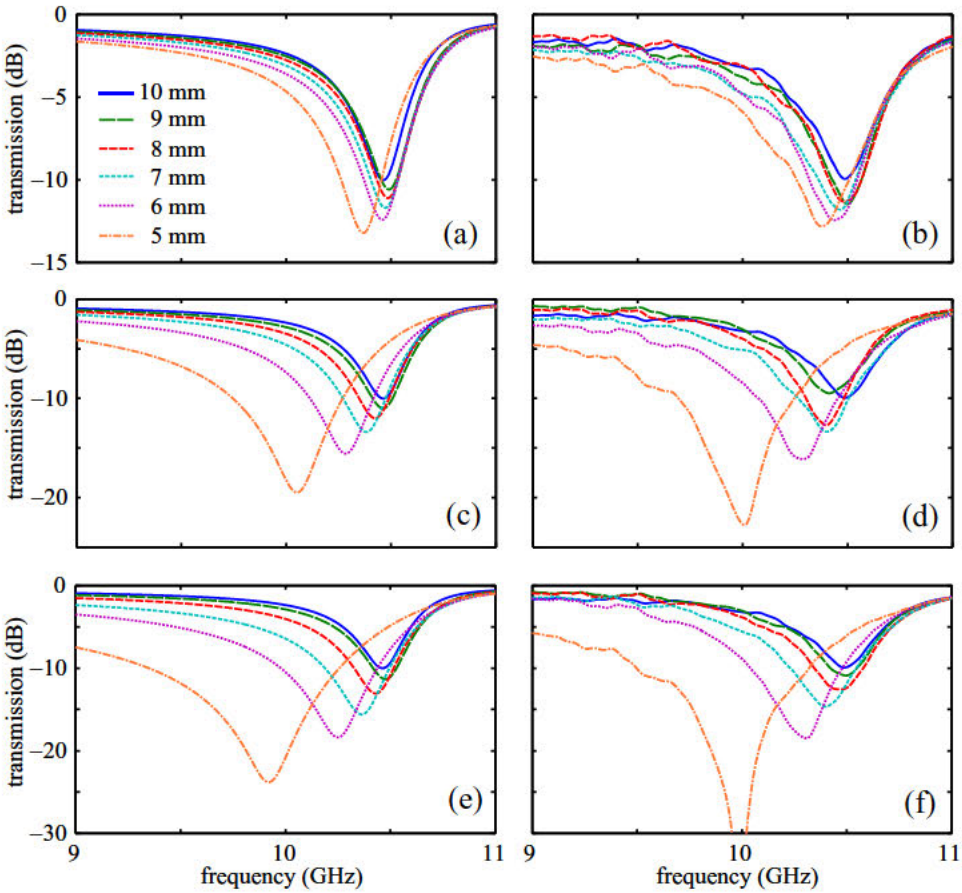

Figure 3. Transmission amplitude profiles for resonator arrays with different lattice constants. (*a*), (*c*), (*e*) Simulation, and (*b*), (*d*), (*f*) experimental results. (*a*), (*b*) a_x varies and $a_y = 10$ mm. (*c*), (*d*) $a_x = 10$ mm and a_y varies. (*e*), (*f*) or a_x and a_y vary. Note the different scales for the three cases.

be expressed as

$$\mathcal{L} = \sum_{u,v}\left[\frac{L}{2}(\dot{Q}_{u,v}^2 + 2\kappa_{h_x}\dot{Q}_{u,v}\dot{Q}_{u+1,v} - 2\kappa_{h_y}\dot{Q}_{u,v}\dot{Q}_{u,v+1}) - \frac{1}{2C}(Q_{u,v}^2 + 2\kappa_{e_x}Q_{u,v}Q_{u+1,v} - 2\kappa_{e_y}Q_{u,v}Q_{u,v+1})\right], \quad (1)$$

where $\kappa_{\{h,e\}}$ are the magnetic and electric coupling coefficients. The coupling effects are considered for only the four nearest neighbouring resonators. The sign difference in the coupled energy terms reflects difference contributions. The coupling coefficients are essentially direction-dependent, as they are determined by the uneven charge and current distributions over coupled resonators [6]. It is known that at the same distance the magnitude of κ_{e_y} is twice that of κ_{e_x}, according to the near-field electric field distribution of an infinitesimal dipole [25]. Furthermore, as opposed to the SRR array [14], the magnetic coupling coefficients κ_{h_x} and κ_{h_y} are not identical, because of the unique orientation of the two magnetic dipoles within a cell. These coefficients can be linked to the lateral lattice constants via [14]

$$\kappa_{h_x} = \kappa_{h_x,0}/a_x^3\,, \quad (2a)$$
$$\kappa_{h_y} = \kappa_{h_y,0}/a_y^3\,, \quad (2b)$$
$$\kappa_{e_x} = \kappa_{e_x,0}/a_x^3\,, \quad (2c)$$
$$\kappa_{e_y} = \kappa_{e_y,0}/a_y^3\,. \quad (2d)$$

Solving the Euler–Lagrange equation [26]

$$\frac{\mathrm{d}}{\mathrm{d}t}\left(\frac{\partial\mathcal{L}}{\partial\dot{Q}_{u,v}}\right) - \frac{\partial\mathcal{L}}{\partial Q_{u,v}} = 0, \quad (3)$$

with the Lagrangian in equation (1) and assuming a plane-wave excitation or $Q_{u,v} = Q_{u\pm1,v} = Q_{u,v\pm1} = |Q|\exp(j\omega t)$, results in the resonance frequency of the array

$$\omega_s = \omega_0\sqrt{\frac{1+\kappa_{e_x}-\kappa_{e_y}}{1+\kappa_{h_x}-\kappa_{h_y}}}, \quad (4)$$

where the resonance frequency of the uncoupled resonator ω_0 equals $1/\sqrt{LC}$. The unknown coefficients can be determined by comparing this solution to the measured or simulated resonance frequency [8].

Figure 4 shows the measured resonance frequencies fitted by the Lagrangian solution, along with the corresponding coupling coefficients. A slight difference in the model and measurement in figure 4(*a*) can be observed, particularly for the case of $a_x = a_y = 5$ mm. This is likely to be from the magnetic dipole coupling in the diagonal direction, which is omitted in the model, and also from the approximation of the coupling coefficients in equation 2. From figure 4(*b*), in the horizontal direction, the magnetic coupling coefficient is slightly larger than the electric counterpart, i.e. $\kappa_{h_x}/\kappa_{e_x} = 1.14$. The

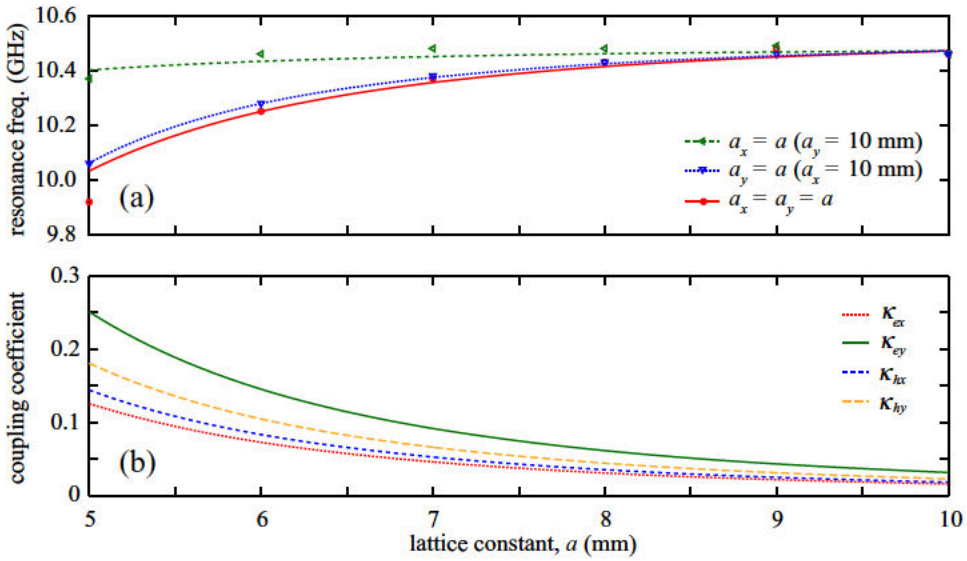

Figure 4. Resonance frequencies and coupling coefficients as a function of the lattice constant. (*a*) Simulated resonance frequencies (dots) fitted by the model (lines) in equation (4). (*b*) Coupling coefficients, $\kappa_{e_x,0} = 15.7\,\text{mm}^3$, $\kappa_{e_y,0} = 31.4\,\text{mm}^3$, $\kappa_{h_x,0} = 18.0\,\text{mm}^3$, $\kappa_{h_y,0} = 22.6\,\text{mm}^3$.

opposing coupling mechanisms yield the net effect that shifts down the resonance slightly, as illustrated in figure 4(*a*). In the vertical direction, $\kappa_{h_y}/\kappa_{e_y} = 0.72$. Hence, the dominant electric dipole coupling causes a redshift in the resonance. The stronger magnetic dipole coupling in the y direction, or $\kappa_{h_y} > \kappa_{h_x}$, can be ascribed to the alignment of the two magnetic dipoles within a single cell. Importantly, it is clear from the results that the ELC resonators still exhibit a significant local magnetic coupling activity, although their magnetic and magnetoelectric responses are suppressed in the far field [2, 3].

3. Longitudinal coupling

3.1. Observation

This section presents a study on the effects of longitudinal coupling in ELC resonators. The unit cell dimensions and constituent materials are similar to those in the previous study in section 2. However, in this study, as shown in figure 5, two identical arrays of ELC resonators are aligned and stacked in the propagation direction with an adjustable distance a_z from 1 to 10 mm with a step size of 1 mm. Between the two arrays, the electric dipoles couple transversely, and the magnetic dipoles couple longitudinally. For the face-to-face stack, the couplings are mainly through free space, whilst for the back-to-face stack a dielectric substrate will greatly influence the electric coupling [27]. The effects from interactions among in-plane resonators are minimized by using relatively large fixed lattice constants of 10 mm for a_x and a_y. This configuration is expected to yield the results that can reasonably reflect the activities of ELC dimers.

Figure 6(*a*) shows the numerically resolved transmission magnitude for the face-to-face array stack with varying separations a_z. At $a_z = 10$ mm, the transmission resonance is only slightly different from the resonance of the single array with the same periods a_x and a_y. It implies that the two

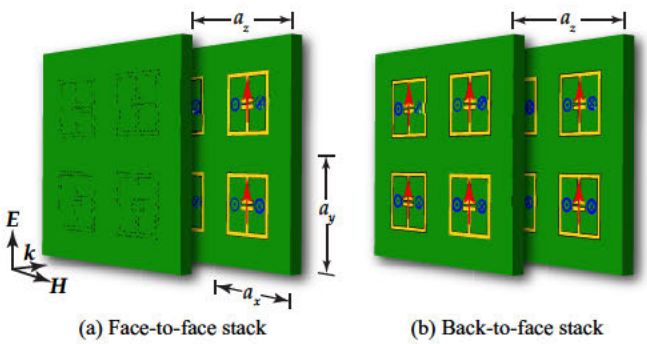

Figure 5. Stacked ELC resonators configured for longitudinal coupling. (*a*) Face-to-face stack and (*b*) back-to-face stack. The lattice constants a_x and a_y are kept constant at 10 mm, whilst a_z, measured between the resonator planes, varies between 1 and 10 mm. The electric dipoles (red arrows) are perpendicular to the resonator gaps, whilst the magnetic dipoles (blue arrows) are normal to the resonator plane.

arrays are weakly coupled. When they are brought closer, the resonance is weakened and then split into two peaks, an indication of the hybridization. Around $a_z = 2$ mm the two resonances degenerate, before being split again into two distant peaks at $a_z = 1$ mm. Noticeably, at $a_z = 1$ mm the lower resonance is much stronger than the higher one. This is because the two electric dipoles in the dimer are in-phase at the lower resonance, and hence preferentially coupled to the excitation [8]. In the case of the back-to-face stack in figure 6(*b*), the resonance splitting can be observed at any distance a_z under investigation without a mode crossing.

Different modes of resonance can be distinguished in the simulation. Figure 7 depicts the electric field distributions around an ELC dimer at resonances. From the field distributions, the symmetric and asymmetric modes of resonance can be observed. In the symmetric mode, the transversal electric dipoles are in phase, as are the longitudinal

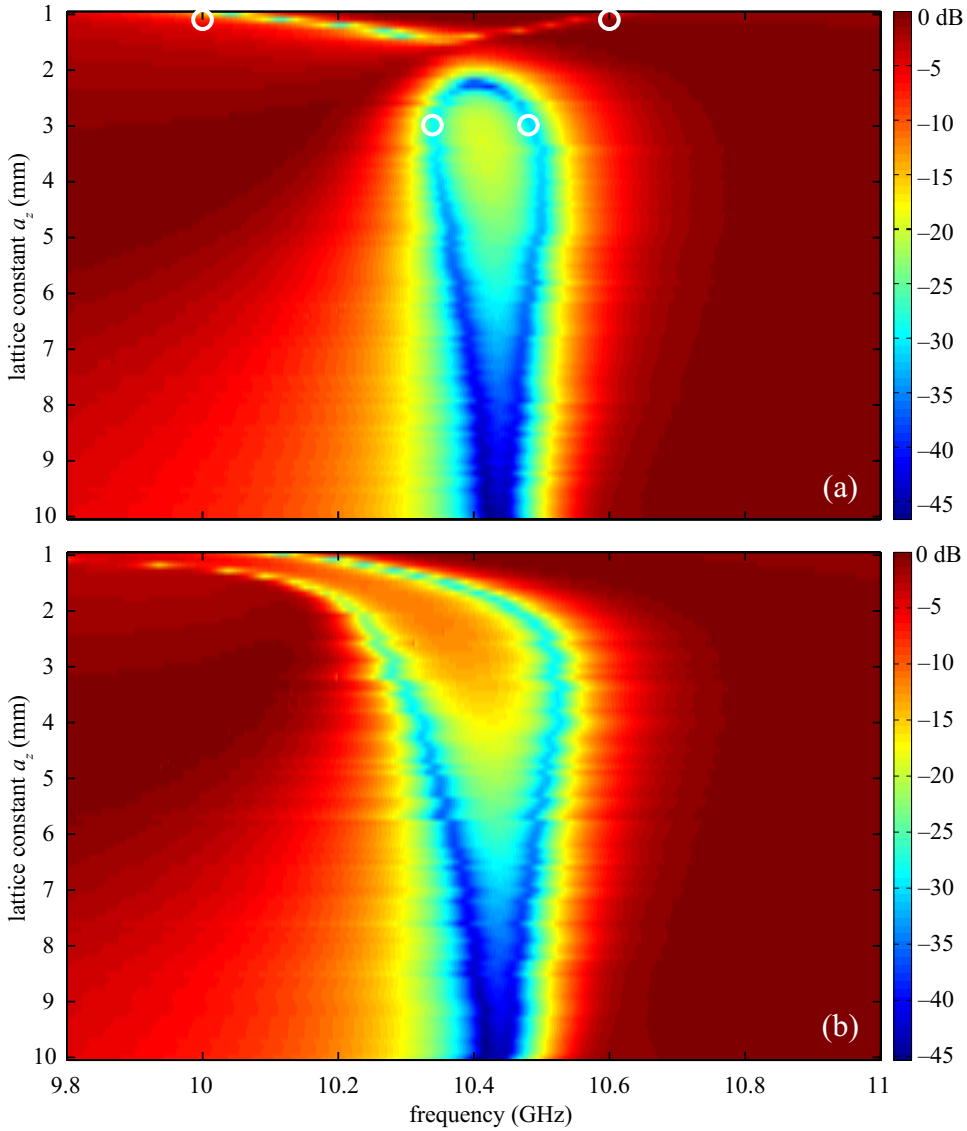

Figure 6. Transmission magnitude of the array stack for a range of a_z. (*a*) Face-to-face stack, and (*b*) back-to-face stack. The loss in the substrate is neglected in the simulation. The white circles in (*a*) indicate the lattice constants and frequencies that are used to produce the field distributions in figure 7.

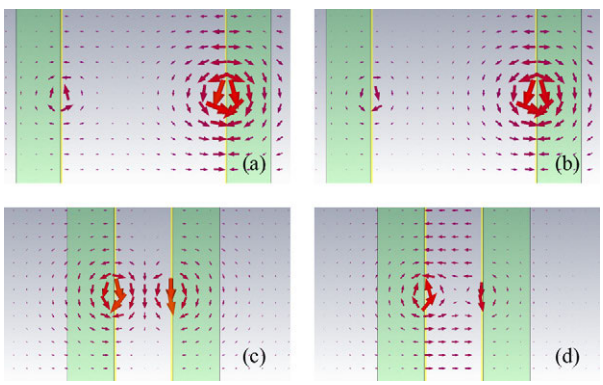

Figure 7. Instantaneous electric field distributions for face-to-face ELC-resonator stack. The yz plane cuts across the gap of each resonator. (*a*), (*b*) $a_z = 3$ mm, and (*c*), (*d*) $a_z = 1$ mm. (*a*) Asymmetric mode at $f_{as} = 10.3$ GHz. (*b*) Symmetric mode at $f_s = 10.5$ GHz. (*c*) Symmetric mode at $f_s = 10.0$ GHz. (*d*) Asymmetric mode at $f_{as} = 10.6$ GHz.

magnetic dipoles. Vice versa, in the asymmetric mode, the electric dipoles are out of phase, as are the magnetic dipoles. Hence, in either case, the effect from electric and magnetic dipole–dipole interactions always counteracts each other. More specifically, in the symmetric mode, the longitudinal magnetic dipole–dipole interaction tends to shift down the resonance, whilst the transversal electric interaction acts in the opposite direction. In the asymmetric mode, the electric dipole interaction tends to shift down the resonance, whilst the magnetic interaction counteracts the effect.

For the face-to-face stack in figure 7, at $a_z = 3$ mm the lower and higher resonances are asymmetric and symmetric, respectively. As for $a_z = 1$ mm, the two modes are swapped. Hence, it can be deduced that at a moderate distance between the resonators in a dimer, i.e. $a_z > 2$ mm, the electric dipole coupling dominantly influences the hybridization. The observable mode crossing and swapping are caused by a high magnetic flux density near to the surface of each resonator.

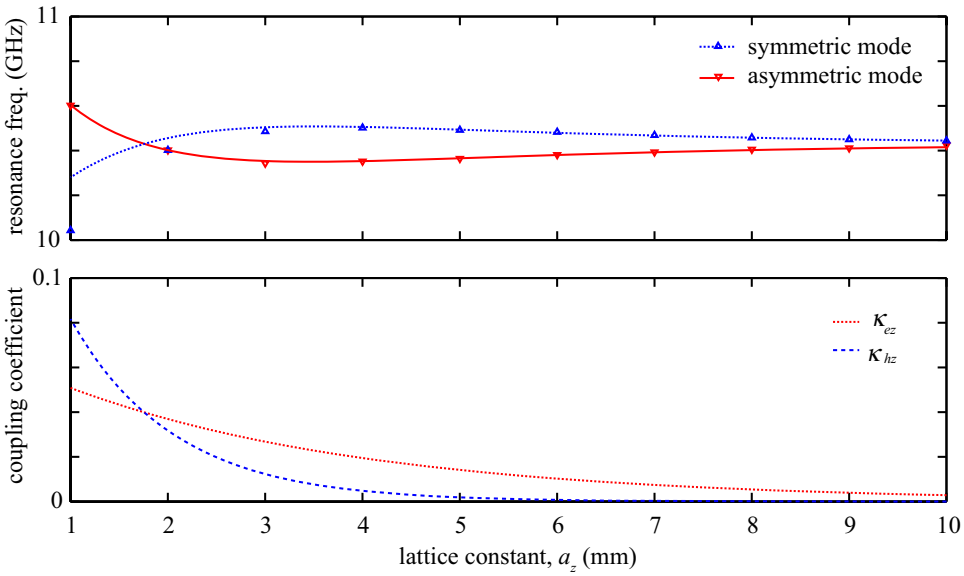

Figure 8. Resonance frequencies and coupling coefficients as a function of the lattice constant. (*a*) Simulated resonance frequencies (dots) fitted by the model (lines) in equation (6*a*). (*b*) Field coupling coefficients, $\kappa_{h_z} = \kappa_{h_z,0}\exp(-m_h a_z)$ and $\kappa_{e_z} = \kappa_{e_z,0}\exp(-m_e a_z)$, where $\kappa_{h_z,0} = 0.21$, $\kappa_{e_z,0} = 0.07$, $m_h = 0.945\,\mathrm{mm}^{-1}$ and $m_e = 0.320\,\mathrm{mm}^{-1}$. The exponential functions and associated values are obtained from observation.

In this case, the electric dipole coupling is dominated by the magnetic coupling. An additional investigation shows that for the back-to-face stack, the lower and higher resonances are asymmetric and symmetric, respectively, at $1\,\mathrm{mm} \leqslant a_z \leqslant 10\,\mathrm{mm}$. In the other words, the electric dipole–dipole interaction always controls the hybridization. The different hybridization behaviour in the back-to-face stack is likely to be from the intermediate dielectric layer that promotes the electric dipole interaction below $a_z = 2\,\mathrm{mm}$. By choosing a thinner substrate it might be possible to restore the mode crossing. However, this case will not be considered in section 3.2.

3.2. Analysis

The analysis in this part emphasizes the coupling in the face-to-face stack, shown in figure 5(*a*). Owing to the large distance among in-plane resonators, the couplings in the lateral directions are negligible. By considering only a pair of stacked resonators, or a dimer, the Lagrangian can be established as [9]

$$\mathcal{L} = \frac{L}{2}(\dot{Q}_1^2 + 2\kappa_{h_z}\dot{Q}_1\dot{Q}_2 + \dot{Q}_2^2) - \frac{1}{2C}(Q_1^2 + 2\kappa_{e_z}Q_1Q_2 + Q_2^2), \tag{5}$$

where κ_{h_z} and κ_{e_z} represent the magnetic and electric coupling coefficients in the propagation direction, respectively. Solving the Euler–Lagrange equation, with $Q_1 = Q_2$ for the symmetric mode ω_s, and $Q_1 = -Q_2$ for the asymmetric mode ω_as, yields

$$\omega_\mathrm{s} = \omega_0\sqrt{\frac{1+\kappa_{e_z}}{1+\kappa_{h_z}}}, \tag{6a}$$

$$\omega_\mathrm{as} = \omega_0\sqrt{\frac{1-\kappa_{e_z}}{1-\kappa_{h_z}}}. \tag{6b}$$

These resolved modes of resonance are similar to the case of SRR dimers or stereometamaterials [5, 9].

Table 1. Coupling coefficients of ELC resonators in different directions. The coefficients are obtained from the analyses in sections 2.2 and 3.2, and are estimated at $a_x = a_y = a_z = 5\,\mathrm{mm}$.

Coupling coefficients	x	y	z
Electric, κ_e	0.126	0.251	0.014
Magnetic, κ_h	0.144	0.180	0.002

The modelled resonance frequencies and the coupling coefficients for the dimer are depicted in figure 8. A small discrepancy between the analytical and numerical models is likely caused by higher-order interactions omitted from the Lagrangian. The two coefficients can be approximated by exponential functions of the distance. The analysis confirms that, depending on the distance, either the electric or magnetic dipole interaction influences the hybridization. For $a_z > 1.8\,\mathrm{mm}$, the electric dipolar coupling dominates the behaviour of ELC dimers. At $a_z \approx 1.8$ where $\kappa_{h_z} = \kappa_{e_z}$, the mode crossing can be observed. As a_z approaches 1 mm, the magnetic coupling coefficient rises significantly and surpasses the electric coupling coefficient, due to the magnetic activity close to the surfaces of the resonators.

Table 1 summarizes the coupling coefficients between ELC resonators in different directions with the same lattice constant. By comparing only the electric coupling coefficients, it is clear that the coupling strength between electric dipoles is largest in the y direction. This result is agreeable with the intermediate near-field radiation pattern of an infinitesimal electric dipole, whose field strength is strongest in the axial direction [25]. The magnetic coupling coefficients suggest that the coupling strength is very small in the direction normal to the resonator plane. The coupling strength becomes considerably large in the other two directions, despite the zero net magnetic flux in an individual ELC resonator.

4. Conclusion

This paper presents a comprehensive investigation on the near-field interactions among ELC resonators. The observed resonance behaviours are analysed using the Lagrangian formalism. It can be concluded that the near-field interaction in the horizontal direction only slightly changes the resonance due to the counteraction between the electric and magnetic couplings. In the vertical direction, the coupling causes a large redshift in the resonance due to in-phase longitudinal electric dipoles. In the case of the ELC-resonator dimer, the resonance hybridization exhibiting symmetric and asymmetric modes can be observed, and the dominating coupling mechanism depends on the distance between the two resonators. It is pointed out that although an ELC resonator does not possess a magnetic or magnetoelectric response to an external field, the induced local magnetic field significantly contributes to the near-field interactions and cannot be neglected. The knowledge derived from this analysis is essential for designing and analysing ELC resonators in various applications.

Acknowledgments

The authors thank Ian Linke, Brandon Pullen, Pavel Simcik and Henry Ho for their technical assistance. This research was supported by the Australian Research Council Discovery Projects funding scheme under Projects DP1095151 and DP120100200. CF acknowledges the ARC Future Fellowship funding scheme under FT100100585.

References

[1] Pendry J B, Holden A J, Robbins D J and Stewart W J 1999 Magnetism from conductors and enhanced nonlinear phenomena *IEEE Trans. Microw. Theory Tech.* **47** 2075–84
[2] Schurig D, Mock J J and Smith D R 2006 Electric-field-coupled resonators for negative permittivity metamaterials *Appl. Phys. Lett.* **88** 041109
[3] Padilla W J, Aronsson M T, Highstrete C, Lee M, Taylor A J and Averitt R D 2007 Electrically resonant terahertz metamaterials: theoretical and experimental investigations *Phys. Rev.* B **75** 041102
[4] Valentine J, Zhang S, Zentgraf T, Ulin-Avila E, Genov D A, Bartal G and Zhang X 2008 Three-dimensional optical metamaterial with a negative refractive index *Nature* **455** 376–9
[5] Liu H, Liu Y M, Li T, Wang S M, Zhu S N and Zhang X 2009 Coupled magnetic plasmons in metamaterials *Physica Status Solidi* b **246** 1397–406
[6] Powell D A, Lapine M, Gorkunov M V, Shadrivov I V and Kivshar Y S 2010 Metamaterial tuning by manipulation of near-field interaction *Phys. Rev.* B **82** 155128
[7] Liu H, Genov D A, Wu D M, Liu Y M, Liu Z W, Sun C, Zhu S N and Zhang X 2007 Magnetic plasmon hybridization and optical activity at optical frequencies in metallic nanostructures *Phys. Rev.* B **76** 073101
[8] Liu N, Liu H, Zhu S and Giessen H 2009 Stereometamaterials *Nature Photon.* **3** 157–62
[9] Powell D A, Hannam K, Shadrivov I V and Kivshar Y S 2011 Near-field interaction of twisted split-ring resonators *Phys. Rev.* B **83** 235420
[10] Liu H, Genov D A, Wu D M, Liu Y M, Steele J M, Sun C, Zhu S N and Zhang X 2006 Magnetic plasmon propagation along a chain of connected subwavelength resonators at infrared frequencies *Phys. Rev. Lett.* **97** 243902
[11] Li T, Ye R X, Li C, Liu H, Wang S M, Cao J X, Zhu S N and Zhang X 2009 Structural-configurated magnetic plasmon bands in connected ring chains *Opt. Express* **17** 11486–94
[12] Liu N, Guo H, Fu L, Kaiser S, Schweizer H and Giessen H 2008 Three-dimensional photonic metamaterials at optical frequencies *Nature Mater.* **7** 31–7
[13] Li T Q, Liu H, Li T, Wang S M, Wang F M, Wu R X, Chen P, Zhu S N and Zhang X 2008 Magnetic resonance hybridization and optical activity of microwaves in a chiral metamaterial *Appl. Phys. Lett.* **92** 131111
[14] Sersic I, Frimmer M, Verhagen E and Koenderink A F 2009 Electric and magnetic dipole coupling in near-infrared split-ring metamaterial arrays *Phys. Rev. Lett.* **103** 213902
[15] Liu R, Degiron A, Mock J J and Smith D R 2007 Negative index material composed of electric and magnetic resonators *Appl. Phys. Lett.* **90** 263504
[16] Karamanos T D, Dimitriadis A T and Kantartzis N V 2012 Compact double-negative metamaterials based on electric and magnetic resonators *IEEE Antennas Wireless Propag. Lett.* **11** 480–3
[17] Tao H, Landy N T, Bingham C M, Zhang X, Averitt R D and Padilla W J 2008 A metamaterial absorber for the terahertz regime: Design, fabrication and characterization *Opt. Express* **16** 7181–8
[18] Cheng Q, Cui T J, Jiang W X and Cai B G 2010 An omnidirectional electromagnetic absorber made of metamaterials *New J. Phys.* **12** 063006
[19] Zhu B, Feng Y, Zhao J, Huang C and Jiang T 2010 Switchable metamaterial reflector/absorber for different polarized electromagnetic waves *Appl. Phys. Lett.* **97** 051906
[20] Chen H T, Padilla W J, Cich M J, Azad A K, Averitt R D and Taylor A J 2009 A metamaterial solid-state terahertz phase modulator *Nature Photon.* **3** 148–51
[21] Withayachumnankul W, Fumeaux C and Abbott D 2011 Planar array of electric-*LC* resonators with broadband tunability *IEEE Antennas Wireless Propag. Lett.* **10** 577–80
[22] Chin J Y, Lu M and Cui T J 2008 Metamaterial polarizers by electric-field-coupled resonators *Appl. Phys. Lett.* **93** 251903
[23] Zhu B, Feng Y, Zhao J, Huang C, Wang Z and Jiang T 2010 Polarization modulation by tunable electromagnetic metamaterial reflector/absorber *Opt. Express* **18** 23196–203
[24] Strikwerda A C, Fan K, Tao H, Pilon D V, Zhang X and Averitt R D 2009 Comparison of birefringent electricsplit-ring resonator and meanderlinestructures as quarter-wave plates at terahertz frequencies *Opt. Express* **17** 136–149
[25] Balanis C A 2005 *Antenna Theory: Analysis and Design* (New York: Wiley-Interscience) 3rd edn
[26] Morin D 2008 *Introduction to Classical Mechanics: With Problems and Solutions* (Cambridge: Cambridge University Press)
[27] Withayachumnankul W, Fumeaux C and Abbott D 2012 Controlling the hybridization in stereometamaterials *Proc. Int. Conf. on Metamaterials, Photonic Crystals and Plasmonics (META'12) (Paris, France)* pp 14–18